Article

Neuron

Chemogenetic Interrogation of a Brain-wide Fear Memory Network in Mice

Highlights

- Contextual fear memories engage a brain-wide network in mice
- In silico deletion of high, but not low, degree nodes disrupts network function
- In vivo chemogenetic silencing of hub nodes impairs fear memory consolidation
- Network-based approaches are useful for understanding brain-behavior relations

Authors

Gisella Vetere, Justin W. Kenney, Lina M. Tran, ..., John Parkinson, Sheena A. Josselyn, Paul W. Frankland

Correspondence

paul.frankland@sickkids.ca

In Brief

Memories are thought to be supported by a broad network of co-active brain regions. Using computational and neuronal silencing approaches, Vetere et al. provide evidence that hub regions within these networks play disproportionately influential roles in memory consolidation.

Vetere et al., 2017, Neuron *94*, 363–374
April 19, 2017
http://dx.doi.org/10.1016/j.neuron.2017.03.037

CellPress

Neuron
Article

Chemogenetic Interrogation of a Brain-wide Fear Memory Network in Mice

Gisella Vetere,[1,7] Justin W. Kenney,[1,7] Lina M. Tran,[1,2] Frances Xia,[1,2] Patrick E. Steadman,[1,3] John Parkinson,[4,5] Sheena A. Josselyn,[1,2,3,6] and Paul W. Frankland[1,2,3,6,8,*]
[1]Program in Neurosciences and Mental Health, The Hospital for Sick Children, Toronto, ON M5G 1X8, Canada
[2]Department of Physiology
[3]Institute of Medical Science
University of Toronto, Toronto, ON M5S 1A8, Canada
[4]Program in Molecular Structure and Function, The Hospital for Sick Children, Toronto, ON M5G 1X8, Canada
[5]Departments of Biochemistry, Computer Science, and Molecular Genetics, University of Toronto, Toronto, ON M5S 1A8, Canada
[6]Department of Psychology, University of Toronto, Toronto, ON M5S 3GM, Canada
[7]These authors contributed equally
[8]Lead Contact
*Correspondence: paul.frankland@sickkids.ca
http://dx.doi.org/10.1016/j.neuron.2017.03.037

SUMMARY

Behavior depends on coordinated activity across multiple brain regions. Within such networks, highly connected hub regions are assumed to disproportionately influence behavioral output, although this hypothesis has not been systematically evaluated. Previously, by mapping brain-wide expression of the activity-regulated gene *c-fos*, we identified a network of brain regions co-activated by fear memory. To test the hypothesis that hub regions are more important for network function, here, we simulated node deletion in silico in this behaviorally defined functional network. Removal of high degree nodes produced the greatest network disruption (e.g., reduction in global efficiency). To test these predictions in vivo, we examined the impact of post-training chemogenetic silencing of different network nodes on fear memory consolidation. In a series of independent experiments encompassing 25% of network nodes (i.e., 21/84 brain regions), we found that node degree accurately predicted observed deficits in memory consolidation, with silencing of highly connected hubs producing the largest impairments.

INTRODUCTION

A predominant view in the nineteenth century was that specific cognitive functions were localized to discrete brain regions. This view has since evolved to one where specific cognitive functions are thought to be supported by the coordinated activity of a distributed network of brain regions, rather than isolated brain regions alone (McIntosh, 1999; Park and Friston, 2013; Sporns, 2012). Graph theory is a branch of mathematics that has been used to analyze such complex networks. Any network consists of nodes (or vertices) connected through links (or edges), with degree centrality describing the number of links per node. Analysis of many real world networks (including social, ecological, protein interaction, gene, finance, and communication networks) reveals that probability distributions for node degree are typically heavy tailed (e.g., scale-free), with low degree nodes being common and high degree nodes being more scarce (Barabási, 2009). However, despite their scarcity, high degree nodes (or "hubs") are thought to exert greater influence on network function by virtue of greater connectivity, and targeting hubs disproportionately impacts the function of real-world networks. For example, in protein interaction networks, experimental deletion of genes coding for high-degree proteins is associated with greater lethality than similar deletion of genes coding for low-degree proteins (Babu et al., 2012, 2014; Jeong et al., 2001).

Network-based approaches have been used to describe large-scale structural (i.e., anatomical) and functional (i.e., co-activation) connections in the brain (Bargmann and Marder, 2013; Bullmore and Sporns, 2012; Chiang et al., 2011; Jarrell et al., 2012; Markov et al., 2014; Oh et al., 2014; Varshney et al., 2011; White et al., 1986). Similar to other networks, probability distributions for node degree are heavy tailed (Bullmore and Bassett, 2011; Rubinov and Sporns, 2010; van den Heuvel et al., 2016). This "small-world" organization is thought to facilitate rapid brain-wide synchronization and information transfer, and, at the same time, this architecture minimizes wiring costs and provides a balance between local processing and global integration (Sporns, 2013). Although brain diseases, including Alzheimer's disease and schizophrenia, are more likely to impact brain regions identified as hubs in human anatomical connectomic analyses (Crossley et al., 2014), systematic manipulation of nodes within a task-relevant network has not been possible to date.

By mapping activity-regulated gene expression induced by memory recall, we recently described a network engaged by contextual fear memory in mice (Wheeler et al., 2013). In this study, we quantified expression of the activity-regulated gene *c-fos* in 84 brain regions after fear memory recall in mice. By computing interregional correlations, we identified collections

of brain regions that were co-activated by memory recall (i.e., a memory network, with nodes representing individual brain regions and edges representing super-threshold functional connections). As expected, the probability distribution for node degree was heavy tailed, and the network contained several high degree hubs including, for example, the CA1 region of the hippocampus and the reuniens thalamic nucleus (Re). To directly test the hypothesis that higher degree nodes exert greater influence on network function, here, we simulated the impact of node deletion on network function using a novel disruption propagation model. We found that deletion of high degree nodes caused the greatest network disruption. We then tested these in silico predictions in vivo by examining the impact of post-training chemogenetic silencing on consolidation of a fear memory. In a series of experiments, we independently probed 25% of network nodes (i.e., 21/84 brain regions). We found that in silico simulation of node deletion accurately predicted observed in vivo data, with silencing of highly connected hubs producing the largest consolidation impairments. This systematic interrogation of an identified, task-relevant network supports the hypothesis that high degree nodes are more crucial for brain function and confirms the predictive value of this network-based approach.

RESULTS

Generation of a Fear Memory Network

Two brain regions are functionally connected when activity in these regions co-varies (Park and Friston, 2013). To measure activity following recall of a fear memory in mice, we previously quantified expression of the activity-regulated gene *c-fos* in 84 brain regions, including regions in the cortex, hippocampus, thalamus, midbrain, cerebral, and hypothalamic nuclei (Table S1). To estimate patterns of functional connectivity, we computed a complete set of interregional correlations. By considering only the strongest correlations, we identified a network of brain regions that were co-activated by memory recall (Figure 1A). In this fear memory functional network, nodes represent individual brain regions and edges represent super-threshold functional connections (Figure 1B) (Wheeler et al., 2013).

This fear memory network displayed several features that were consistent with both theoretical predictions and experimental observations. First, similar to other brain networks (van den Heuvel et al., 2016), the probability distribution for node degree was heavy tailed (Figure S1A). Second, the network was highly clustered, such that a small-world network model approximated the clustering distribution (Figure S1B). Third, several high degree nodes within the network corresponded to regions with established roles in fear memory (e.g., CA1, Re) (Tanaka et al., 2014; Xu and Südhof, 2013) (Figure S1C). Importantly, these features were observed when we used alternate correlation coefficients to generate the network, as well as more or less conservative thresholds for functional connections (Wheeler et al., 2013). Furthermore, equivalent patterns of functional connections were observed when another activity-related gene, *zif268*, was quantified in the same brains (Wheeler et al., 2013).

We additionally generated two types of comparison network. For the first network, we quantified Fos expression in the same 84 brain regions in a control condition, run in parallel with the fear conditioned mice. In this control condition, mice were treated identically to the fear conditioned group except that they did not receive a shock during training (Wheeler et al., 2013) (Figures 1C and 1D). Similar to the fear memory network, the probability distribution for node degree was non-Gaussian, with the nucleus accumbens shell (AcbSh), ventromedial thalamic nucleus (VM), and anteroventral thalamic nucleus (AV) having the most connections (Figure S1D). However, compared to the memory network, this control network was less dense, reflecting reduced interactions between brain regions in the absence of fear memory expression.

The second type of network was generated to evaluate corresponding anatomical connections (using structural data from the Allen Brain Atlas connectomic dataset; Oh et al., 2014). Because the functional (i.e., fear memory and control) and anatomical networks were generated in fundamentally different ways, we used two methods to generate corresponding anatomical networks: (1) an anatomical network thresholded at the same p value as the functional network and (2) an anatomical network with the same density (i.e., number of edges) as the functional network (see STAR Methods) (Figures S1E and S1F). As expected, these networks contained a subset of hub-like regions, with the caudate putamen (CPu), claustrum (Cl), and agranular insular cortex, ventral part (AIV) having the most connections (Figures S1G and S1H).

The fear memory network appeared to differ qualitatively from both the control and anatomical networks. Consistent with this, degree centrality was not correlated between the fear memory network and either the control or anatomical networks, indicating that hubs in the fear memory network differed from hubs in these other networks. Comparing the fear memory and the control networks, this was the case whether we used equivalent thresholds to generate the networks ($r = 0.045$, $p = 0.68$) or we matched networks in terms of density ($r = 0.072$, $p = 0.51$) (Figures S1I and S1J). Comparing the fear memory and the anatomical networks, this was the case whether we used equivalent thresholds to generate the networks ($r = 0.078$, $p = 0.52$) or we matched networks in terms of density ($r = 0.024$, $p = 0.84$) (Figures S1K and S1L). The lack of correspondence between the fear memory and control networks suggests that interactions between regions vary across conditions (i.e., fear memory versus control). The lack of correspondence between the fear memory and anatomical networks suggests that patterns of behaviorally determined functional connections provide important information beyond underlying structural connections (Mišić et al., 2016).

In Silico Node Deletion

Within these types of networks, high degree nodes (or hubs) are thought to exert greater influence on network function by virtue of their greater connectivity. We first developed an in silico approach to model the effects of node removal on global network properties. The brain is highly interconnected and inactivation of any single node is likely to exert effects beyond its immediate neighborhood (Goshen et al., 2011; Grayson et al., 2016; Liu et al., 2012; Lohani et al., 2016; Otchy et al., 2015). Therefore, in contrast to network analyses in which a node is

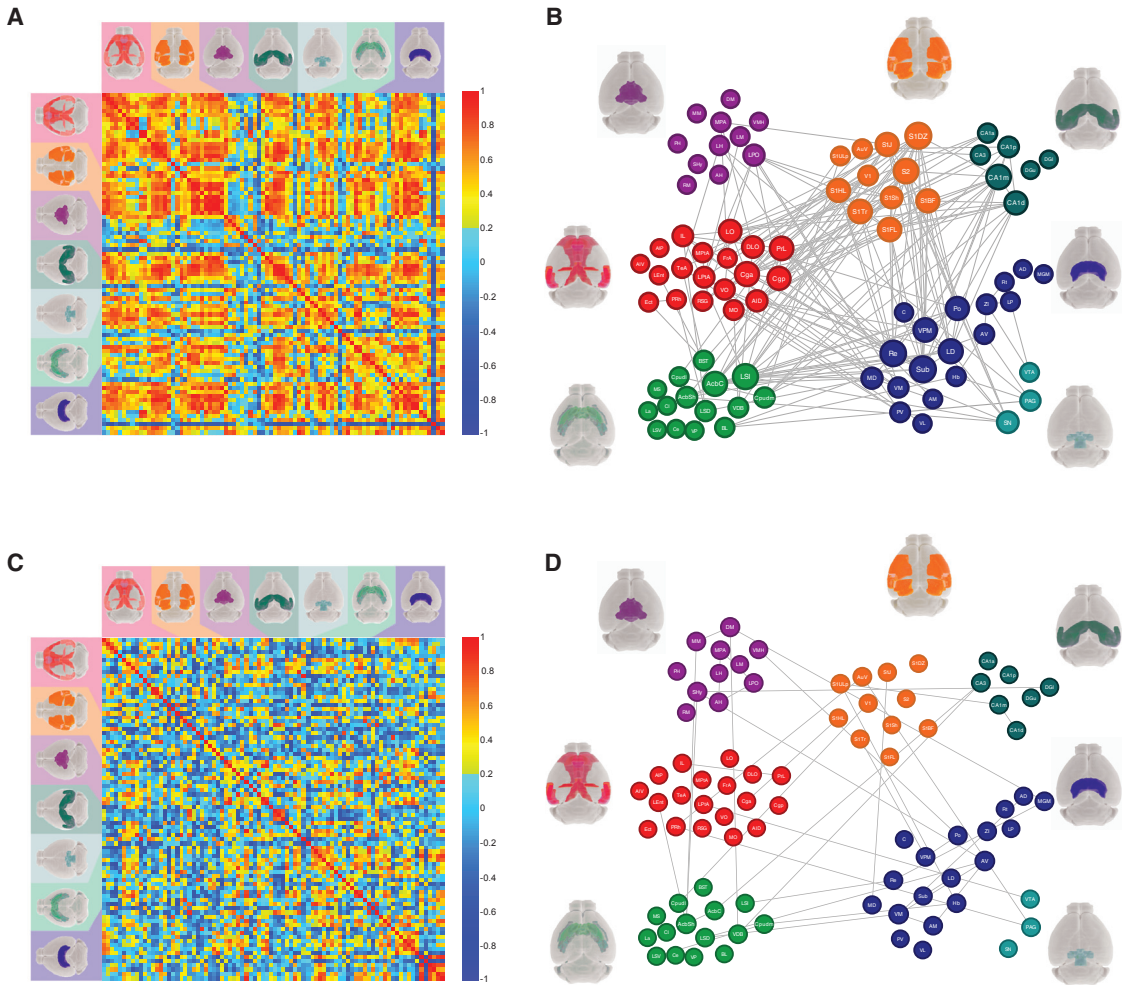

Figure 1. Identification and Characterization of a Fear Memory Network

(A) Matrix showing interregional correlations for Fos expression following fear memory recall. The axes correspond to 84 brain regions (listed in Table S1) organized by major brain division (red, association cortex; purple, hypothalamus; orange, sensory cortex; teal, hippocampus; blue, thalamus; turquoise, midbrain; green, cerebral nuclei). The colors reflect the strength of correlation (scale, right).

(B) Resulting network graph with nodes grouped by major brain divisions. The node size is proportional to its degree (i.e., number of connections). The connections correspond to the above threshold correlations (Pearson's $r >= 0.83$, $p < 0.01$).

(C) Matrix showing interregional correlations for Fos expression for mice in the control condition. The axes correspond to 84 brain regions (listed in Table S1) organized by major brain division (red, association cortex; purple, hypothalamus; orange, sensory cortex; teal, hippocampus; blue, thalamus; turquoise, midbrain; green, cerebral nuclei). The colors reflect the strength of correlation (scale, right).

(D) Resulting network graph with nodes grouped by major brain divisions. The node size is proportional to its degree (i.e., number of connections). The connections correspond to the above threshold correlations (Pearson's $r >= 0.83$, $p < 0.01$).

simply removed from a network while global network measures are recalculated, we modeled the effects of inhibiting individual brain regions (nodes) in the fear memory network by propagating the effect of inactivation beyond a given node along the contours of the connectome. This disruption propagation model (DPM) directly exploits the functional connectome associated with a specific behavior. Related approaches have been used to model cascading failures in electric grid networks (Crucitti et al., 2004).

In the DPM, an individual node and its associated edges are deleted from the network. In order to propagate this disruption beyond the deleted node's neighborhood, the weights of all adjacent edges are adjusted (1) proportionally to the weight of the deleted edge and (2) inversely proportional to their own neighboring edges. These steps are iterated through the network until edge weights no longer change (Figure S2). The resulting network is then thresholded after propagation to produce the disrupted network. The model has two tunable parameters: (1) the number of times any edge can be updated and (2) the threshold applied following edge updating to generate the disrupted network. Exploration of these parameters indicated that combining one edge update with a threshold matching that used for initial network generation yielded high information content (i.e., Shannon's Entropy; Figures S3A–S3D), and, therefore, we used these parameters in all our subsequent analyses.

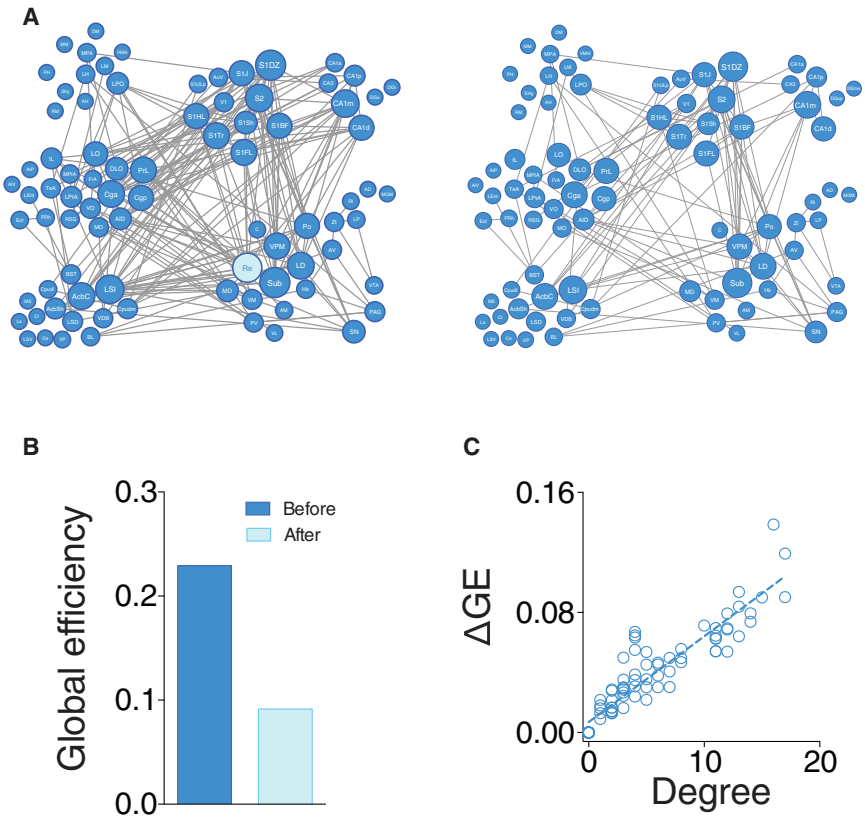

Figure 2. In Silico Silencing of Individual Network Nodes

(A) Fear memory network before (left) and after (right) application of the DPM targeting Re (light blue).

(B) Network global efficiency decreases after application of DPM targeting the Re.

(C) Positive correlation between degree and change in global efficiency (ΔGE) following DPM application.

We applied our disruption propagation model to each node to simulate the effect of inactivation on overall network function. To measure the impact of inactivating individual nodes, we compared the network before and after disruption and calculated the change in global efficiency (ΔGE) (Figures 2A and 2B, example for Re shown) and giant component size (ΔGC) for each node. For the fear memory network, we found that changes in global efficiency were correlated with node degree (r = 0.92, $p < 0.001$; Figure 2C), with inactivation of high degree nodes associated with greater reductions in global efficiency than similar inactivation of low degree nodes. An equivalent pattern of results was observed for changes in giant component size (r = 0.65, $p < 0.01$; Figures S3E and S3F). As expected, reductions in global efficiency and giant component using the DPM were greater in magnitude than reductions in these measures following simple node deletion (Figures S4A and S4B). Furthermore, ΔGE and ΔGC were more strongly correlated with degree centrality using the DPM compared to simple node deletion (for simple deletion: ΔGE, r = 0.66, $p < 0.001$ and ΔGC, r = 0.20, p = 0.067; Figures S4C and S4D).

In Vivo Node Silencing

We next tested whether the predicted in silico deficits would be observed in vivo. To do this, we chronically silenced brain regions identified in our network analysis and examined the impact on memory consolidation. To chronically suppress neural activity in targeted brain regions, we virally expressed the inhibitory DREADD (designer receptor exclusively activated by designer drugs), hM4Di (Armbruster et al., 2007), using long-term expressing replication-defective herpes simplex viruses (HSVs). This strategy offers two key advantages. First, HSVs are neurotropic, infecting predominantly excitatory neurons and not glia (Cole et al., 2012; Rashid et al., 2016; Yiu et al., 2014). Second, unlike optogenetic manipulations, DREADDs allow chronic silencing of neuronal activity (i.e., days to weeks; Jain et al., 2013) by administering the hM4Di ligand clozapine-N-oxide (CNO) in drinking water.

We previously showed that bath application of the hM4Di ligand, CNO, hyperpolarized infected neurons and suppressed spiking in ex vivo whole cell patch clamp recording experiments (Richards et al., 2014). In order to further verify that hM4Di expression decreases neuronal activity in vivo, we microinjected HSV-hM4Di into the anterior cingulate cortex. At 3 days later (when expression of hM4Di began), mice were given continuous home cage access to CNO (or its vehicle [VEH]) in their drinking water to silence infected neurons. At 3 days later, we trained mice in contextual fear conditioning at different Zeitgeber times (ZTs), with ZT0 corresponding to lights on and ZT12 corresponding to lights off. At 90 min following training, mice were perfused and expression of the activity-dependent immediate early gene, *c-fos*, in neurons expressing hM4Di was examined (Figure 3A). The proportion of hM4Di-expressing neurons expressing Fos was reduced following CNO treatment (main treatment effect: $F_{1,39}$ = 20.76, $p < 0.0001$), indicating that the combination of hM4Di and CNO administered in drinking water reduced neuronal activity in vivo (Figure 3B). Importantly, the degree of Fos reduction was similar at all ZTs (treatment × ZT interaction: $F_{1,39}$ = 0.15, p = 0.93), consistent with previous studies showing that (1) drinking is reduced, but not absent, during the inactive phase of the light-dark cycle in mice (Gordon et al., 1986) and (2) systemically administered CNO suppresses neuronal firing hM4Di-expressing neurons for up to 9 hr (Armbruster et al., 2007).

Using the same procedures, we additionally assessed whether similar CNO treatment (i.e., 3 days) decreases neuronal activity in hM4Di-infected neurons in other brain regions (CA1, laterodorsal thalamic nucleus [LD] and medial geniculate

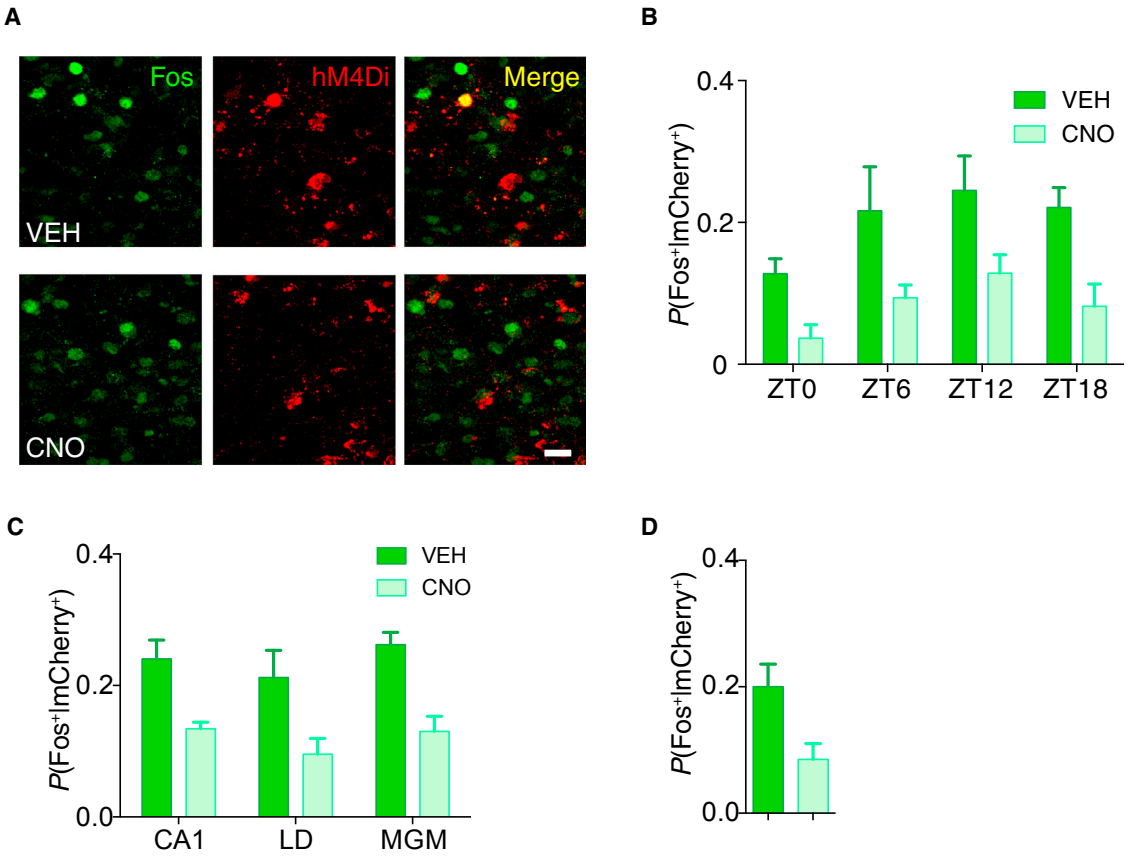

Figure 3. Chemogenetic Inhibition Suppresses Neuronal Activation

(A) Anterior cingulate cortex neurons expressing hM4Di-mCherry (red) show lower levels of Fos (green) following contextual fear conditioning in mice treated with CNO (lower) versus VEH (upper) in drinking water. Note overlap of hM4Di with Fos (yellow) in VEH-treated mice, but not CNO-treated mice. The scale bar represents 20 μm.

(B) Probability of Fos expression in neurons expressing hM4Di-mCherry following fear conditioning was reduced in mice treated with CNO (versus VEH) in drinking water, regardless of ZT of training.

(C) Probability of Fos expression in neurons expressing hM4Di-mCherry following fear conditioning was reduced in mice treated with CNO (versus VEH) in drinking water, regardless of site of infection.

(D) Prolonged CNO treatment (10 days) reduces probability of Fos expression in neurons expressing hM4Di-mCherry in CA1 following fear conditioning. All of the data represent mean ± SEM.

nucleus, medial part [MGM]). At 90 min following training (at ZT6), the proportion of hM4Di-expressing neurons expressing Fos was reduced in CNO-treated mice in all brain regions (treatment effect: $F_{1,18}$ = 17.78, p < 0.0005) (Figure 3C). The magnitude of this reduction was similar in all regions (treatment × region interaction: $F_{2,18}$ = 0.06, p = 0.94), suggesting that there are no obvious regional variations in the efficiency of CNO-induced neural suppression. Furthermore, in a separate experiment, Fos expression was similarly reduced in infected neurons in CA1 following extended CNO treatment (i.e., 10 days, matching the time course of the main experiments, below) (t_6 = 2.64, p < 0.05) (Figure 3D).

Targeting 21 Different Regions in Independent Experiments

To systematically examine the relationship between a region's node degree and necessity in memory consolidation, we targeted 21 different regions from our network in a series of independent experiments (i.e., these experiments encompassed 25% of network nodes) (Figure 4A; Table S2). Targeted regions included low, medium, and high degree nodes (node degree range 0–17) and encompassed the anterior-posterior extent of the network (including regions in association and sensory cortices, thalamus, hippocampus, cerebral, and hypothalamic nuclei). For each region, mice were bilaterally microinjected with HSV-hM4Di into the target region and trained in contextual fear conditioning 3 days later. Immediately following training, mice were given continuous home cage access to CNO or VEH in their drinking water and tested 10 days later (for each region, N's ranged 6–10 for CNO and VEH) (Figure 4B). Across all experiments, a total of 344 mice were tested (VEH, n = 174 and CNO, n = 170). Within each region, ~2,000 neurons were infected (range 900–3,000) (Figure 5A). To assess differences in freezing between CNO- and VEH-treated mice, we conducted permutation tests, and then to control for multiple tests (across

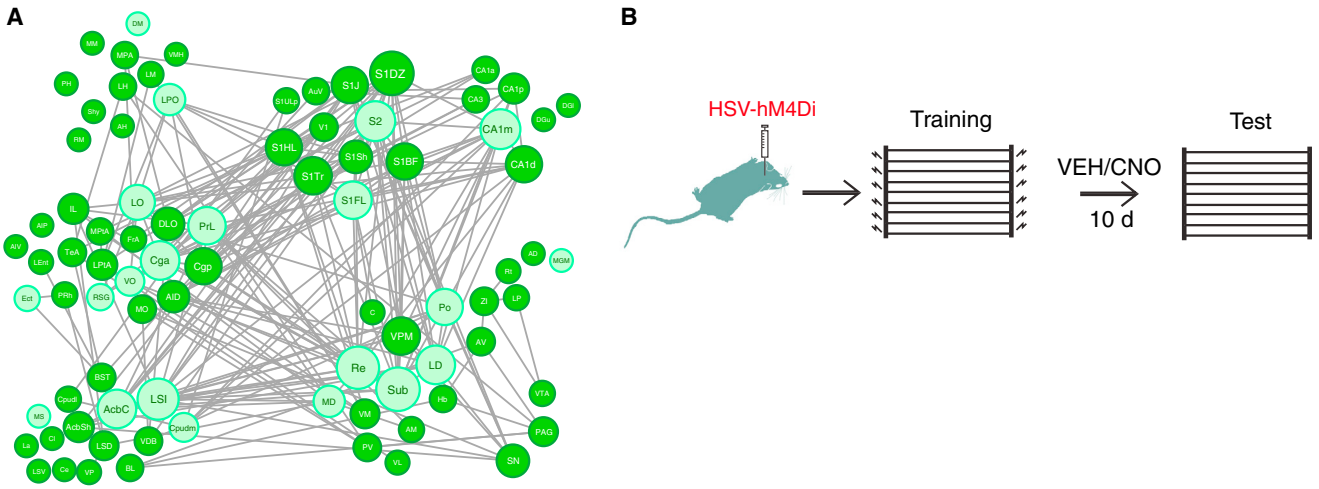

Figure 4. In Vivo Silencing of Individual Network Nodes

(A) There were 21 brain regions that were chemogenetically silenced in independent experiments.

(B) HSV-hM4Di was bilaterally microinjected into 21 different brain regions. The mice were trained in contextual fear conditioning and tested 10 days later. After training, the mice received CNO or VEH in drinking water.

21 experiments), we adjusted p values using false discovery rate (FDR) of 5% (Benjamini et al., 2001). Using this criterion, chronic suppression of neuronal activity in 4/21 brain regions targeted impaired consolidation (Figure 5B). These regions were the CA1 region of the hippocampus, lateral septal nucleus (LSI), LD, and Re. Importantly, the combination of hM4Di and CNO administration appears to be necessary for the observed behavioral effects. Compared to VEH, CNO treatment did not impair consolidation in mice infected with the control virus in CA1 (t_{14} = 0.51, p = 0.62) (Figure S5A).

Correspondence between In Silico and In Vivo Node Silencing

We next examined the extent to which our in silico predictions of the effects of node silencing corresponded to the observed in vivo consolidation deficits. Reductions in freezing (consolidation deficits) following in vivo chemogenetic silencing correlated with reductions in global efficiency following in silico node deletion (r = 0.61, p < 0.01) (Figure 6A; see also Table S3). Similarly, reductions in freezing following regional in vivo chemogenetic silencing correlated with reductions in giant component following in silico node deletion (r = 0.56, p < 0.01) (Figure S5B). This correspondence between DPM-based predictions and in vivo observations was insensitive to variations in network generation. Applying the DPM to either higher confidence (thresholded at p < 0.005) or lower confidence (thresholded at p < 0.05) networks, produced similar correspondence between in silico reductions in global efficiency and in vivo data (high, r = 0.58, p < 0.01 and low, r = 0.46, p < 0.05), indicating that the predictive power of the DPM is insensitive to network thresholding. These results suggest that inactivation of higher degree nodes is associated with greater consolidation deficits. Consistent with this conclusion, we found that a region's "hubness" predicted the observed consolidation deficits following silencing. This was the case for degree centrality (r = 0.57, p < 0.01; Figure S5C), as well as alternate measures of centrality including node strength (r = 0.57, p < 0.01), closeness (r = 0.56, p < 0.01), communicability (r = 0.45, p < 0.05), eigenvector (r = 0.53, p < 0.05), and Katz centrality (r = 0.52, p < 0.05).

We next contrasted our DPM-based predictions to predictions produced by either simple node removal or the cascading failure model, a related approach that has been used to model electrical grid failure (Crucitti et al., 2004). The DPM was superior to both simple node removal (correlation between ΔGE and Δfreezing: r = 0.45, p < 0.05) and the cascading failure model (correlation between $\alpha_{critical}$ and Δfreezing: r = 0.41, p = 0.064) (Figures S5D and S5E), suggesting that features of the DPM more faithfully mimic the impact of localized inactivation on brain network function.

In our experiments, we microinjected a fixed volume of HSV-hM4Di into the different regions of interest. As the volume of targeted regions varied across brain regions, it is possible that observed consolidation deficits are related to the proportion of the target region infected by our viral vector. However, the volume of targeted regions did not correlate with observed deficits (r = 0.09, p = 0.70) (Figure S5F).

Control and Anatomical Networks Do Not Predict Consolidation Deficits

The present results indicate that our fear memory network model successfully predicted the effectiveness of chemogenetic silencing and are consistent with the idea that inactivation of higher degree nodes is associated with greater consolidation deficits. However, there are alternate possibilities. For example, it is possible that basal network interactions between these same brain regions during other behavioral states predict the observed consolidation deficits. Alternatively, the underlying anatomical connections between the same brain regions might predict the observed consolidation deficits. A third possibility is that differences in regional activation levels (relative to the control condition) account for the observed in vivo results.

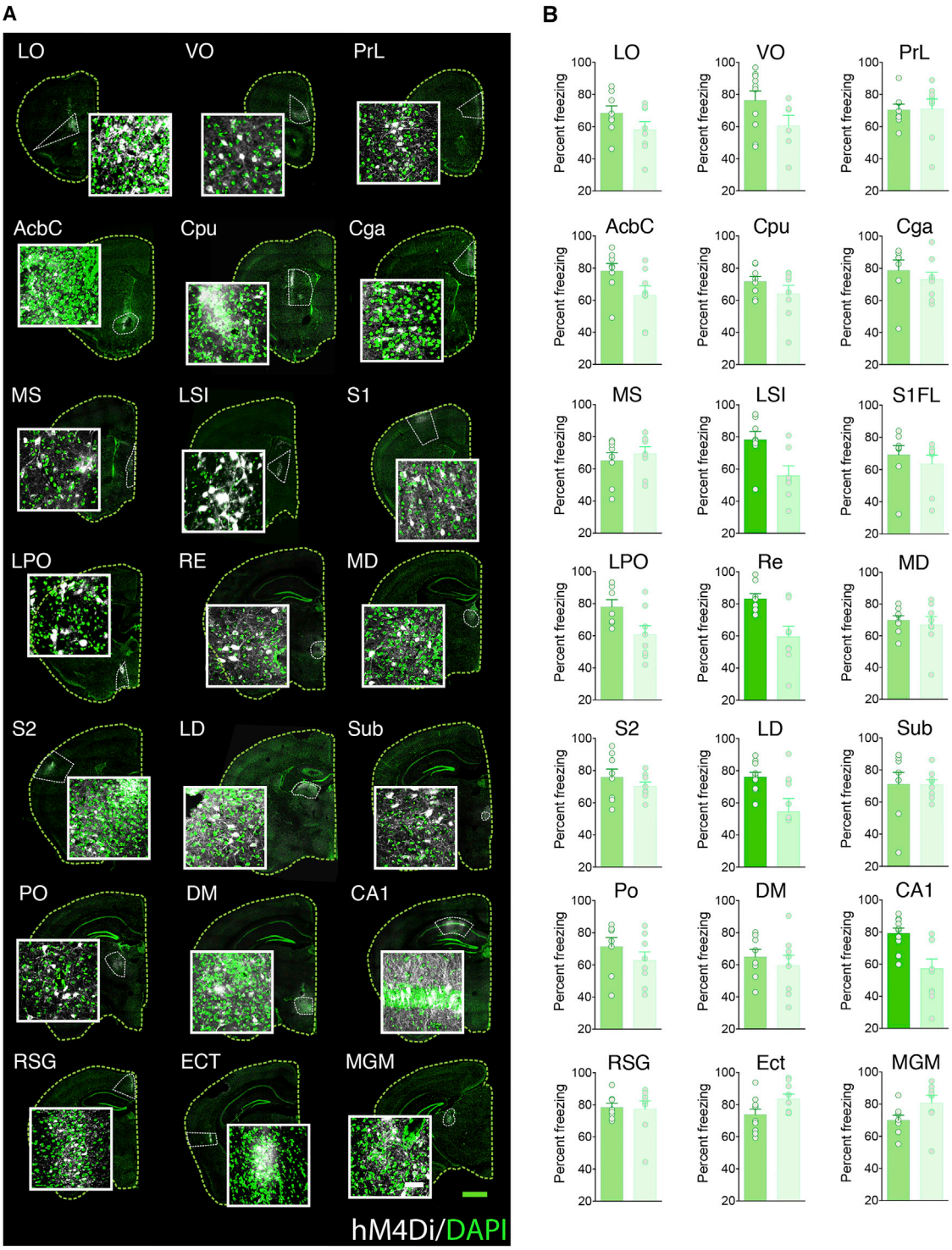

Figure 5. Effects of Chemogenetic Silencing of 21 Different Brain Regions

(A) Bilateral microinjection of HSV-hM4Di produced localized transgene expression (white) in the targeted 21 brain regions. The targeted regions are outlined (white dotted lines). The scale bar (green) represents 1 mm. The insets show high magnification of infected regions. The inset scale bar (white) represents 50 μm. (B) Contextual fear memory (percent freezing) in mice treated with VEH (dark green) or CNO (light green) in targeted brain regions. The dots represent freezing scores for individual mice. The statistically reliable differences (after FDR correction) are highlighted by the darker green bar (LSI, Re, LD, and CA1). All of the data represent mean ± SEM.

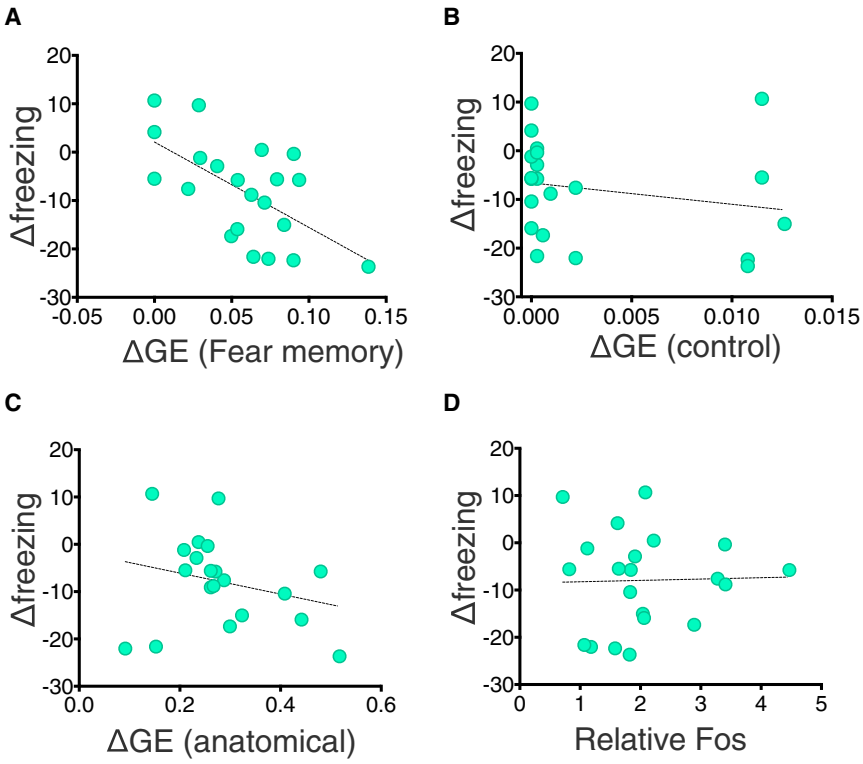

Figure 6. In Silico Analysis Predicts In Vivo Observations

(A) Reductions in ΔGE following application of the DPM in silico (applied to the fear memory network) predict reductions in freezing (Δfreezing) following chemogenetic silencing observed in vivo.

(B) Changes in global efficiency (ΔGE) following application of the DPM in silico (applied to the control network) do not predict reductions in freezing (Δfreezing) following chemogenetic silencing observed in vivo.

(C) Changes in global efficiency (ΔGE) following application of the DPM in silico (applied to the anatomical network) do not predict reductions in freezing (Δfreezing) following chemogenetic silencing observed in vivo.

(D) Differences in regional Fos expression (normalized to untrained control group) did not predict reductions in freezing (Δfreezing) observed in vivo.

In order to test the first possibility, we asked whether the topological organization observed in the control network predicted the effectiveness of chemogenetic silencing. As in the fear memory network, we applied the DPM to the control network and calculated changes in global efficiency. We found that changes in global efficiency did not predict consolidation deficits. This was the case regardless of whether we used an equivalent thresholding criteria compared to the fear memory network (r = 0.21, p = 0.36; Figure 6B) or matched control network density with the fear memory network (r = 0.36, p = 0.11; Figure S6A).

To test the second possibility, we asked whether the topological organization observed in anatomical networks predicted the effectiveness of chemogenetic silencing. As in the fear memory network, we applied the DPM to the anatomical networks and calculated changes in global efficiency. We found that changes in global efficiency did not predict consolidation deficits. This was the case regardless of whether we used an equivalent thresholding criteria compared to the fear memory network (r = 0.25, p = 0.28; Figure 6B) or matched anatomical network density with the fear memory network (r = 0.048, p = 0.84; Figure S6C).

Finally, we found that relative activation levels (i.e., Fos counts normalized to a control group) did not predict consolidation deficits (r = 0.027, p = 0.91; Figure 6D).

DISCUSSION

By quantifying expression of the activity-regulated gene *c-fos*, we previously identified a network of brain regions that were co-activated by recall of a fear memory in mice (Wheeler et al., 2013). Graph theoretical analysis identified several highly connected hub regions within this functional network, and, here, we tested the hypothesis that these hubs would play more influential roles in memory consolidation compared to non-hub regions. First, we developed the DPM to simulate removal of individual brain regions in silico. As expected, removal of high degree nodes produced greater network disruption (reductions in global efficiency and giant component size) than removal of low degree nodes. Second, we examined the impact of silencing individual brain regions on fear memory consolidation in vivo. We found that inactivation of higher degree nodes was associated with greater consolidation deficits than similar inactivation of low degree nodes. Network-based approaches have previously been used to analyze large-scale structural (i.e., anatomical) and functional (i.e., co-activation) connections in the brain. However, formal interrogation of these networks using invasive interventions has not been conducted. The current study indicates that network-based approaches may provide a predictive framework that may be useful in identifying novel brain-behavior relationships.

In our network generation (Wheeler et al., 2013), two regions were determined to be functionally connected when activity in one region was statistically dependent upon activity in another region (McIntosh, 1999; Park and Friston, 2013). In previous studies, hemodynamic (fMRI) or electrophysiological estimates of regional and/or neuronal activity have been used to estimate patterns of functional connectivity, and resulting functional networks, in humans and experimental animals (Sporns and Betzel, 2016). The use of an activity-regulated gene marker, such as Fos, to measure regional patterns of activation in mice necessarily means that the present network generation differs in two important ways. First, Fos expression was measured 90 min following memory testing (in order to match the time course of elevated Fos protein following sustained neuronal activation). While functional connections may be defined across a range of timescales (McIntosh, 1999), this timescale is longer than that

used in fMRI or electrophysiological studies. Correlations in Fos expression therefore likely incompletely capture the richness of all interregional interactions (e.g., although the amygdala is known to be important for fear learning, it was not identified as an important node in our network). They are useful in detecting co-activation of brain regions when it is sustained over minutes, but are insensitive to coupling that may occur over shorter timescales (e.g., interregional coupling of oscillations). It is additionally worth noting that relatively small populations of neurons may robustly influence network activity (e.g., Witten et al., 2010), and such contributions may also be underestimated using the current approach. Second, post-mortem assessment of Fos provides a single indication of activation (rather than a time series) per region per mouse, and, therefore, functional connections are estimated by computing co-variance across, rather than within, mice. While both within and between subject co-variance can be used to estimate functional connections (Grady et al., 2003; McIntosh, 1999), within subject co-variance is more typically used in fMRI or electrophysiological studies.

Despite these differences, we were able to use our fear memory network in an unbiased manner to predict which brain regions within this network are important for consolidation of a fear memory. Consistent with the in silico analyses, the most pronounced deficits in fear memory consolidation occurred when activity in higher degree nodes was suppressed post training. Importantly, neither the corresponding control nor anatomical networks accurately predicted the observed consolidation deficits. With respect to the control network, this suggests that network interactions among these same brain regions vary according to behavioral state (in this case, fear memory versus control). With respect to the anatomical network, this emphasizes that analyses of patterns of behaviorally determined functional connections provide important information beyond underlying structural connections. Indeed, while anatomical networks constrain and influence resulting functional networks, there is often considerable topographical divergence (e.g., Mišić and Sporns, 2016).

The importance of hubs for network function has previously been assessed in a wide range of biological (Babu et al., 2012, 2014; Jeong et al., 2001) and non-biological complex networks including the internet (Albert et al., 2000), electricity grid (Buldyrev et al., 2010), and financial networks (Haldane and May, 2011). However, systematic, node-by-node interrogation of brain networks has not previously been conducted, even in model organisms with well-defined and tractable connectomes such as *c elegans*. The current study confirms that hubs play disproportionately important roles, at least in a network engaged by contextual fear memory in mice. Our findings are broadly consistent with a previous meta-analysis finding that highly connected brain regions are more likely to be impacted in a range of brain disorders (Crossley et al., 2014). In the future, two developments may further refine this general approach in rodents and allow broader application. First, the development of improved methods for brain-wide quantification of activity-regulated gene expression will allow for the generation of more accurate activity maps (Renier et al., 2016; Ye et al., 2016). Further refinements will allow phenotyping of cells expressing activity-regulated genes and therefore segregation of signals by cell type and/or neurotransmitter content (Romanov et al., 2016). Second, the development of imaging approaches that allow neuronal activity to be tracked in real time across large expanses of tissue (e.g., based on voltage, Ca^{2+} or hemodynamic signals) will improve temporal resolution (Ahrens et al., 2013; Ferenczi et al., 2016; Gong et al., 2015; Mohajerani et al., 2013). This will permit use of time series data for network generation and analysis and, additionally, make it possible to track interregional coupling over shorter timescales.

We found that post-training chemogenetic inhibition of four (out of 21) regions impaired memory consolidation. These regions were CA1, Re, LSI, and LD. Of these, two were unsurprising. Previous studies have established roles for both the CA1 region of the hippocampus and the Re in the consolidation and expression of contextual fear memories. For example, fear conditioning activates CA1 neurons (Beck and Fibiger, 1995), and inhibition of CA1 neurons during training, following training, or during retrieval impairs contextual fear memories (Fanselow, 2000). The Re has been shown to influence fear memory expression. Inhibition of prefrontal inputs to Re or Re projections increases generalized freezing in non-trained contexts. Conversely, activation of Re neurons reduced generalized freezing in non-trained contexts (Xu and Südhof, 2013). Nonetheless, previous studies did not evaluate whether neural activity in the Re is important for fear memory consolidation, as we showed here.

The observations that post-training inhibition of either LSI or LD impaired consolidation of contextual fear conditioning are novel. However, there is anatomical and functional data that plausibly implicate these regions in circuits supporting fear-related behaviors and/or mnemonic processing. The LD has dense reciprocal connectivity with the hippocampus and retrosplenial cortex (Aggleton et al., 2016). This region has been implicated in cortical-hippocampal-thalamic circuits involved in recognition memory (Aggleton et al., 2016), and LD inactivation disrupts hippocampal place representations and spatial learning (Mizumori et al., 1994; van Groen et al., 2002). The LSI receives strong inputs from the hippocampus and amygdala and sends projections to midbrain and brainstem regions implicated in behavioral and autonomic reactions to threatening stimuli (Swanson and Cowan, 1979). The LSI is activated by threatening stimuli (Beck and Fibiger, 1995) and mediates, for example, anxiogenic responses and enhanced fear induced by social defeat (Guzmán et al., 2013). Furthermore, inactivation of hippocampal-LSI projections impairs expression of context-reward associations (Luo et al., 2011). Consistent with the present study, this suggests that hippocampal-LSI interactions play a broader role in processing contextual memories.

We developed a new model to simulate the impact of node removal and generate predictions for the in vivo experiments. Most crucially, in this model, the impact of node deletion (and loss of associated edges) was propagated through the network, beyond the node's immediate neighborhood. This particular feature of the DPM was based on many recent observations that localized brain perturbations alter activity in remote brain regions (e.g., Goshen et al., 2011; Grayson et al., 2016; Liu et al., 2012; Lohani et al., 2016; Otchy et al., 2015). For example, prolonged optogenetic inhibition of the CA1 region of the

hippocampus during fear memory recall induces hyper-activation of the anterior cingulate cortex (Goshen et al., 2011). Similarly, optogenetic stimulation of VTA dopaminergic neurons in rats alters brain-wide activation of both non-dopaminergic and dopaminergic circuits, as measured by fMRI (Lohani et al., 2016). Finally, and perhaps most relevant to the approach outlined here, chemogenetic inhibition of the amygdala alters cortex-wide patterns of resting state functional connectivity in the monkey (Grayson et al., 2016).

Compared to simple node deletion, the DPM provided better predictions of the observed consolidation deficits following localized regional neuronal suppression. This suggests that features of the DPM (e.g., mutual dependence of activity in connected brain regions) more faithfully mimic the impact of localized inactivation on brain network function. The DPM also outperformed a conceptually related cascading failure model that has been used to model failures in electricity grids and the internet (Crucitti et al., 2004). In the cascading failure model, the effects of node deletion extend beyond adjacent edges by redistributing loads network wide. Critically, in the cascading failure model, there is a tolerance parameter that defines the change in load that any individual node can sustain before adjacent edges are impacted. Since the DPM performed better than the cascading failure model, this suggests that the concept of node overload may not be as relevant to brain networks.

STAR★METHODS

Detailed methods are provided in the online version of this paper and include the following:

- KEY RESOURCES TABLE
- CONTACT FOR REAGENT AND RESOURCE SHARING
- EXPERIMENTAL MODEL AND SUBJECT DETAILS
  - Experimental Animals
- METHOD DETAILS
  - Network analysis
  - Disruption propagation model
  - Anatomical network analysis
  - Cascading failure model
  - Virus
  - Surgery
  - Contextual fear training and testing
  - CNO treatment
  - Verifying viral infections
  - In vivo assessment of chemogenetic inhibition
  - Immunohistochemistry
- QUANTIFICATION AND STATISTICAL ANALYSIS
  - Fos level quantification
  - Permutation testing
- DATA AND SOFTWARE AVAILABILITY

SUPPLEMENTAL INFORMATION

Supplemental Information includes six figures and three tables and can be found with this article online at http://dx.doi.org/10.1016/j.neuron.2017.03.037.

AUTHOR CONTRIBUTIONS

P.W.F., G.V., and J.W.K. designed the experiments. G.V., L.M.T., and F.X. conducted the behavioral experiments; J.W.K., P.E.S., and J.P. developed the disruption propagation model and conducted graph theoretical analyses; and G.V. and F.X. conducted the immunohistochemical analyses. P.W.F. supervised the project and P.W.F., G.V., J.W.K., S.A.J., and J.P. wrote the paper.

ACKNOWLEDGMENTS

We thank Leonardo Restivo and Anne Wheeler for their technical input at various stages of this project. This work was supported by the Canadian Institutes of Health Research (CIHR) grants to P.W.F. (FDN143227) and S.A.J. (MOP74650) and a Natural Sciences and Engineering Research Council (NSERC) grant to J.P. (RGPIN-2014-06664). J.W.K. was supported by a long-term fellowship from Human Frontiers Science Program (LT000759/2014). P.W.F. and S.A.J. are senior fellows in the Child Brain & Development Program and the Brain, Mind & Consciousness programs, respectively, at the Canadian Institute for Advanced Research (CIFAR).

Received: September 6, 2016
Revised: January 26, 2017
Accepted: March 27, 2017
Published: April 19, 2017

REFERENCES

Aggleton, J.P., Pralus, A., Nelson, A.J., and Hornberger, M. (2016). Thalamic pathology and memory loss in early Alzheimer's disease: moving the focus from the medial temporal lobe to Papez circuit. Brain *139*, 1877–1890.

Ahrens, M.B., Orger, M.B., Robson, D.N., Li, J.M., and Keller, P.J. (2013). Whole-brain functional imaging at cellular resolution using light-sheet microscopy. Nat. Methods *10*, 413–420.

Albert, R., Jeong, H., and Barabasi, A.L. (2000). Error and attack tolerance of complex networks. Nature *406*, 378–382.

Armbruster, B.N., Li, X., Pausch, M.H., Herlitze, S., and Roth, B.L. (2007). Evolving the lock to fit the key to create a family of G protein-coupled receptors potently activated by an inert ligand. Proc. Natl. Acad. Sci. USA *104*, 5163–5168.

Babu, M., Vlasblom, J., Pu, S., Guo, X., Graham, C., Bean, B.D., Burston, H.E., Vizeacoumar, F.J., Snider, J., Phanse, S., et al. (2012). Interaction landscape of membrane-protein complexes in Saccharomyces cerevisiae. Nature *489*, 585–589.

Babu, M., Arnold, R., Bundalovic-Torma, C., Gagarinova, A., Wong, K.S., Kumar, A., Stewart, G., Samanfar, B., Aoki, H., Wagih, O., et al. (2014). Quantitative genome-wide genetic interaction screens reveal global epistatic relationships of protein complexes in Escherichia coli. PLoS Genet. *10*, e1004120.

Barabási, A.L. (2009). Scale-free networks: a decade and beyond. Science *325*, 412–413.

Bargmann, C.I., and Marder, E. (2013). From the connectome to brain function. Nat. Methods *10*, 483–490.

Beck, C.H., and Fibiger, H.C. (1995). Conditioned fear-induced changes in behavior and in the expression of the immediate early gene c-fos: with and without diazepam pretreatment. J. Neurosci. *15*, 709–720.

Benjamini, Y., and Hochberg, Y. (1995). Controlling the false discovery rate: A practical and powerful approach to multiple testing. J. R. Stat. Soc. Ser. A Stat. Soc. *57*, 289–300.

Benjamini, Y., Drai, D., Elmer, G., Kafkafi, N., and Golani, I. (2001). Controlling the false discovery rate in behavior genetics research. Behav. Brain Res. *125*, 279–284.

Buldyrev, S.V., Parshani, R., Paul, G., Stanley, H.E., and Havlin, S. (2010). Catastrophic cascade of failures in interdependent networks. Nature *464*, 1025–1028.

Bullmore, E.T., and Bassett, D.S. (2011). Brain graphs: graphical models of the human brain connectome. Annu. Rev. Clin. Psychol. *7*, 113–140.

Bullmore, E., and Sporns, O. (2012). The economy of brain network organization. Nat. Rev. Neurosci. *13*, 336–349.

Butts, C.T. (2008). Social network analysis with sna. Journal of Statistical Software *24*, 1–51.

Chiang, A.S., Lin, C.Y., Chuang, C.C., Chang, H.M., Hsieh, C.H., Yeh, C.W., Shih, C.T., Wu, J.J., Wang, G.T., Chen, Y.C., et al. (2011). Three-dimensional reconstruction of brain-wide wiring networks in Drosophila at single-cell resolution. Curr. Biol. *21*, 1–11.

Cole, C.J., Mercaldo, V., Restivo, L., Yiu, A.P., Sekeres, M.J., Han, J.H., Vetere, G., Pekar, T., Ross, P.J., Neve, R.L., et al. (2012). MEF2 negatively regulates learning-induced structural plasticity and memory formation. Nat. Neurosci. *15*, 1255–1264.

Crossley, N.A., Mechelli, A., Scott, J., Carletti, F., Fox, P.T., McGuire, P., and Bullmore, E.T. (2014). The hubs of the human connectome are generally implicated in the anatomy of brain disorders. Brain *137*, 2382–2395.

Crucitti, P., Latora, V., and Marchiori, M. (2004). Model for cascading failures in complex networks. Phys. Rev. E Stat. Nonlin. Soft Matter Phys. *69*, 045104.

Csardi, G., and Nepusz, T. (2006). The igraph software package for complex network research. InterJournal. Complex Syst. *1696*, 1–9.

Fanselow, M.S. (2000). Contextual fear, gestalt memories, and the hippocampus. Behav. Brain Res. *110*, 73–81.

Ferenczi, E.A., Zalocusky, K.A., Liston, C., Grosenick, L., Warden, M.R., Amatya, D., Katovich, K., Mehta, H., Patenaude, B., Ramakrishnan, C., et al. (2016). Prefrontal cortical regulation of brainwide circuit dynamics and reward-related behavior. Science *351*, aac9698.

Gong, Y., Huang, C., Li, J.Z., Grewe, B.F., Zhang, Y., Eismann, S., and Schnitzer, M.J. (2015). High-speed recording of neural spikes in awake mice and flies with a fluorescent voltage sensor. Science *350*, 1361–1366.

Gordon, M.N., Osterburg, H.H., May, P.C., and Finch, C.E. (1986). Effective oral administration of 17 beta-estradiol to female C57BL/6J mice through the drinking water. Biol. Reprod. *35*, 1088–1095.

Goshen, I., Brodsky, M., Prakash, R., Wallace, J., Gradinaru, V., Ramakrishnan, C., and Deisseroth, K. (2011). Dynamics of retrieval strategies for remote memories. Cell *147*, 678–689.

Grady, C.L., McIntosh, A.R., and Craik, F.I. (2003). Age-related differences in the functional connectivity of the hippocampus during memory encoding. Hippocampus *13*, 572–586.

Grayson, D.S., Bliss-Moreau, E., Machado, C.J., Bennett, J., Shen, K., Grant, K.A., Fair, D.A., and Amaral, D.G. (2016). The rhesus monkey connectome predicts disrupted functional networks resulting from pharmacogenetic inactivation of the amygdala. Neuron *91*, 453–466.

Guzmán, Y.F., Tronson, N.C., Jovasevic, V., Sato, K., Guedea, A.L., Mizukami, H., Nishimori, K., and Radulovic, J. (2013). Fear-enhancing effects of septal oxytocin receptors. Nat. Neurosci. *16*, 1185–1187.

Hagberg, A.A., Schult, D.A., and Swart, P.J. (2008). Exploring network structure, dynamics, and function using NetworkX. Proceedings of the 7th Python in Science Conference, pp. 11–15.

Haldane, A.G., and May, R.M. (2011). Systemic risk in banking ecosystems. Nature *469*, 351–355.

Hausser, J., and Strimmer, K. (2009). Entropy inference and the James-Stein estimator, with application to nonlinear gene association networks. J. Mach. Learn. Res. *10*, 1469–1484.

Jain, S., Ruiz de Azua, I., Lu, H., White, M.F., Guettier, J.M., and Wess, J. (2013). Chronic activation of a designer G(q)-coupled receptor improves β cell function. J. Clin. Invest. *123*, 1750–1762.

Jarrell, T.A., Wang, Y., Bloniarz, A.E., Brittin, C.A., Xu, M., Thomson, J.N., Albertson, D.G., Hall, D.H., and Emmons, S.W. (2012). The connectome of a decision-making neural network. Science *337*, 437–444.

Jeong, H., Mason, S.P., Barabási, A.L., and Oltvai, Z.N. (2001). Lethality and centrality in protein networks. Nature *411*, 41–42.

Liu, X., Ramirez, S., Pang, P.T., Puryear, C.B., Govindarajan, A., Deisseroth, K., and Tonegawa, S. (2012). Optogenetic stimulation of a hippocampal engram activates fear memory recall. Nature *484*, 381–385.

Lohani, S., Poplawsky, A.J., Kim, S.G., and Moghaddam, B. (2016). Unexpected global impact of VTA dopamine neuron activation as measured by opto-fMRI. Mol. Psychiatry *22*, 585–594.

Luo, A.H., Tahsili-Fahadan, P., Wise, R.A., Lupica, C.R., and Aston-Jones, G. (2011). Linking context with reward: a functional circuit from hippocampal CA3 to ventral tegmental area. Science *333*, 353–357.

Markov, N.T., Ercsey-Ravasz, M.M., Ribeiro Gomes, A.R., Lamy, C., Magrou, L., Vezoli, J., Misery, P., Falchier, A., Quilodran, R., Gariel, M.A., et al. (2014). A weighted and directed interareal connectivity matrix for macaque cerebral cortex. Cereb. Cortex *24*, 17–36.

McIntosh, A.R. (1999). Mapping cognition to the brain through neural interactions. Memory *7*, 523–548.

Mišić, B., and Sporns, O. (2016). From regions to connections and networks: new bridges between brain and behavior. Curr. Opin. Neurobiol. *40*, 1–7.

Mišić, B., Betzel, R.F., de Reus, M.A., van den Heuvel, M.P., Berman, M.G., McIntosh, A.R., and Sporns, O. (2016). Network-level structure-function relationships in human neocortex. Cereb. Cortex *26*, 3285–3296.

Mizumori, S.J., Miya, D.Y., and Ward, K.E. (1994). Reversible inactivation of the lateral dorsal thalamus disrupts hippocampal place representation and impairs spatial learning. Brain Res. *644*, 168–174.

Mohajerani, M.H., Chan, A.W., Mohsenvand, M., LeDue, J., Liu, R., McVea, D.A., Boyd, J.D., Wang, Y.T., Reimers, M., and Murphy, T.H. (2013). Spontaneous cortical activity alternates between motifs defined by regional axonal projections. Nat. Neurosci. *16*, 1426–1435.

Oh, S.W., Harris, J.A., Ng, L., Winslow, B., Cain, N., Mihalas, S., Wang, Q., Lau, C., Kuan, L., Henry, A.M., et al. (2014). A mesoscale connectome of the mouse brain. Nature *508*, 207–214.

Otchy, T.M., Wolff, S.B., Rhee, J.Y., Pehlevan, C., Kawai, R., Kempf, A., Gobes, S.M., and Ölveczky, B.P. (2015). Acute off-target effects of neural circuit manipulations. Nature *528*, 358–363.

Park, H.J., and Friston, K. (2013). Structural and functional brain networks: from connections to cognition. Science *342*, 1238411.

Paxinos, G., and Franklin, K.B.J. (2004). The Mouse Brain in Stereotaxic Coordinates (Gulf Professional Publishing).

Rashid, A.J., Yan, C., Mercaldo, V., Hsiang, H.L., Park, S., Cole, C.J., De Cristofaro, A., Yu, J., Ramakrishnan, C., Lee, S.Y., et al. (2016). Competition between engrams influences fear memory formation and recall. Science *353*, 383–387.

Renier, N., Adams, E.L., Kirst, C., Wu, Z., Azevedo, R., Kohl, J., Autry, A.E., Kadiri, L., Umadevi Venkataraju, K., Zhou, Y., et al. (2016). Mapping of brain activity by automated volume analysis of immediate early genes. Cell *165*, 1789–1802.

Richards, B.A., Xia, F., Santoro, A., Husse, J., Woodin, M.A., Josselyn, S.A., and Frankland, P.W. (2014). Patterns across multiple memories are identified over time. Nat. Neurosci. *17*, 981–986.

Romanov, R.A., Zeisel, A., Bakker, J., Girach, F., Hellysaz, A., Tomer, R., Alpar, A., Mulder, J., Clotman, F., Keimpema, E., et al. (2016). Molecular interrogation of hypothalamic organization reveals distinct dopamine neuronal subtypes. Nat. Neurosci. *20*, 176–188.

Rubinov, M., and Sporns, O. (2010). Complex network measures of brain connectivity: uses and interpretations. Neuroimage *52*, 1059–1069.

Shannon, P., Markiel, A., Ozier, O., Baliga, N.S., Wang, J.T., Ramage, D., Amin, N., Schwikowski, B., and Ideker, T. (2003). Cytoscape: a software environment for integrated models of biomolecular interaction networks. Genome Res. *13*, 2498–2504.

Sporns, O. (2012). From simple graphs to the connectome: networks in neuroimaging. Neuroimage *62*, 881–886.

Sporns, O. (2013). Network attributes for segregation and integration in the human brain. Curr. Opin. Neurobiol. *23*, 162–171.

Sporns, O., and Betzel, R.F. (2016). Modular brain networks. Annu. Rev. Psychol. *67*, 613–640.

Swanson, L.W., and Cowan, W.M. (1979). The connections of the septal region in the rat. J. Comp. Neurol. *186*, 621–655.

Tanaka, K.Z., Pevzner, A., Hamidi, A.B., Nakazawa, Y., Graham, J., and Wiltgen, B.J. (2014). Cortical representations are reinstated by the hippocampus during memory retrieval. Neuron *84*, 347–354.

van den Heuvel, M.P., Bullmore, E.T., and Sporns, O. (2016). Comparative connectomics. Trends Cogn. Sci. *20*, 345–361.

van Groen, T., Kadish, I., and Wyss, J.M. (2002). The role of the laterodorsal nucleus of the thalamus in spatial learning and memory in the rat. Behav. Brain Res. *136*, 329–337.

Varshney, L.R., Chen, B.L., Paniagua, E., Hall, D.H., and Chklovskii, D.B. (2011). Structural properties of the Caenorhabditis elegans neuronal network. PLoS Comput. Biol. *7*, e1001066.

Wheeler, A.L., Teixeira, C.M., Wang, A.H., Xiong, X., Kovacevic, N., Lerch, J.P., McIntosh, A.R., Parkinson, J., and Frankland, P.W. (2013). Identification of a functional connectome for long-term fear memory in mice. PLoS Comput. Biol. *9*, e1002853.

White, J.G., Southgate, E., Thomson, J.N., and Brenner, S. (1986). The structure of the nervous system of the nematode Caenorhabditis elegans. Philos. Trans. R. Soc. Lond. B Biol. Sci. *314*, 1–340.

Witten, I.B., Lin, S.C., Brodsky, M., Prakash, R., Diester, I., Anikeeva, P., Gradinaru, V., Ramakrishnan, C., and Deisseroth, K. (2010). Cholinergic interneurons control local circuit activity and cocaine conditioning. Science *330*, 1677–1681.

Xu, W., and Südhof, T.C. (2013). A neural circuit for memory specificity and generalization. Science *339*, 1290–1295.

Ye, L., Allen, W.E., Thompson, K.R., Tian, Q., Hsueh, B., Ramakrishnan, C., Wang, A.C., Jennings, J.H., Adhikari, A., Halpern, C.H., et al. (2016). Wiring and molecular features of prefrontal ensembles representing distinct experiences. Cell *165*, 1776–1788.

Yiu, A.P., Mercaldo, V., Yan, C., Richards, B., Rashid, A.J., Hsiang, H.L., Pressey, J., Mahadevan, V., Tran, M.M., Kushner, S.A., et al. (2014). Neurons are recruited to a memory trace based on relative neuronal excitability immediately before training. Neuron *83*, 722–735.

STAR★METHODS

KEY RESOURCES TABLE

REAGENT or RESOURCE	SOURCE	IDENTIFIER
Antibodies		
Rabbit polyclonal anti-c-Fos	Santa Cruz Biotechnology	Cat#SC-52; RRID: AB_2106783
Bacterial and Virus strains		
HSV-EF1α-hM4Di-mCherry	McGovern Institute for Brain Research at MIT Viral Core facility or produced in our lab	https://mcgovern.mit.edu/technology/viral-core-facility
HSV-EF1α-GFP	McGovern Institute for Brain Research at MIT Viral Core facility or produced in our lab	https://mcgovern.mit.edu/technology/viral-core-facility
Chemicals, Peptides, and Recombinant Proteins		
Clozapine-N-oxide (CNO)	Toronto Research Chemicals	Cat#C587520
4'6'-diamidino-2-phenylindole (DAPI)	Vectashield	CAS:28718-90-3
Dimethyl sulfoxide (DMSO)	Sigma	CAS:67-68-5
Deposited Data		
Raw and analyzed data	This paper	Dryad: 86337
Experimental Models: Organisms/Strains		
Mouse: C57BL/6N	Taconic Bioscience	C57BL/6NTac
Mouse: 129Svev	Taconic Bioscience	129S6/SvEvTac
Software and Algorithms		
R v3.2.2	CRAN@R-project	http://cran.r-project.org/web/packages/sna/index.html
igraph v1.0.1	Csardi and Nepusz, 2006	http://igraph.org/r/
Entropy v1.2.1	Hausser and Strimmer, 2009	http://cran.r-project.org/web/packages/sna/index.html
sna v2.3.2	Butts, 2008	http://cran.r-project.org/web/packages/sna/index.html
Python v2.7.11	Python Software Foundation	https://www.python.org
Networkx v1.11	Hagberg et al., 2008	http://networkx.readthedocs.io/en/networkx-1.11/
Adobe Illustrator C6	Adobe	http://www.adobe.com/ca/products/illustrator.html
Freeze frame	Actimetrics	http://actimetrics.com/products/freezeframe/
Fiji (ImageJ)	ImageJ	https://fiji.sc
Cytoscape v3.2.1	Shannon et al., 2003	http://www.cytoscape.org
GraphPad Prism 5	GraphPad Software	http://www.graphpad.com/scientific-software/prism/
Disruption propagation model	This paper	Dryad: 86337
Cascading failure model	Crucitti et al., 2004	Dryad: 86337

CONTACT FOR REAGENT AND RESOURCE SHARING

Further information and requests for resources and reagents should be directed to and will be fulfilled by the Lead Contact, Paul Frankland (paul.frankland@sickkids.ca).

EXPERIMENTAL MODEL AND SUBJECT DETAILS

All procedures were conducted in accordance with policies of the Hospital for Sick Children Animal Care Committee and conformed to both Canadian Council on Animal Care (CCAC) and National Institutes of Health (NIH) Guidelines on Care and Use of Laboratory.

Experimental Animals

Male (8–9-week old) wild-type mice were used in all experiments. Mice were the F1 generation derived from crossing 129Svev [129] and C57BL/6N [C57] parents. Mice were weaned at 21 d, then housed 4–5 mice per cage. The housing room was maintained on a 12 h–12 hr light-dark cycle, with lights on during the day.

Cages of mice were randomly assigned to 21 different experimental groups (target brain regions). Each group was further divided into 2 treatment groups (6-12 mice per group) that received either CNO or VEH. All mice in one cage were assigned to the same treatment group (as all mice in the same cage consumed drinking water containing either CNO or VEH).

METHOD DETAILS

Network analysis

The fear network was derived from previously published Fos count data from 84 brain regions following recall of contextual fear memory, tested 36 days following training (Wheeler et al., 2013). Inter-regional Pearson correlations were computed and a threshold of $p < 0.01$ (two-sided) was applied. We also examined lower and higher confidence networks with thresholds of $p < 0.05$, and $p < 0.005$, respectively. Positive correlations with p values below the threshold were included as edges in the resulting networks. A control network was also generated from mice that were treated identically, but did not receive shocks during training (Wheeler et al., 2013). This control network was thresholded using either the same p value ($p < 0.01$, two-sided) or to yield approximately the same number of edges (i.e., equal density) as the fear memory network. Graph theoretical analysis and unweighted centrality measures were calculated using the NetworkX toolbox (version 1.11) in Python 2.7.11 (Hagberg et al., 2008). Networks were visualized using Cytoscape (version 3.2.1) (Shannon et al., 2003).

Disruption propagation model

To examine the effects of network node inactivation we developed a model to simulate the effect of node inactivation in a functional connectome. Typically, the effect of removing a node on the global efficiency or size of the largest connected component (giant component) on network function is performed by removing all edges associated with a node followed by recalculating global efficiency and giant component size. However, brain region inactivation is likely to have effects beyond its immediate neighborhood to other brain regions, so we developed a model to approximate this spreading disruption.

We applied an update rule to edge weights associated with a network that is iterated until the weights in the network no longer change. In the first step, all the edges associated with a specific node are set to zero. The node strength is then calculated for each node at time t, defined as

$$n_i(t) = \sum_j e_{ij}(t),$$

where e_{ij} is the edge weight between nodes i and j. Next, the change in node strength is calculated as

$$\Delta n_i(t) = n_i(t-1) - n_i(t).$$

Edge weights are then updated according to the following rule:

$$e_{ij}(t+1) = e_{ij}(t)\left(1 - \frac{\Delta n_i(t) + \Delta n_j(t)}{n_i(t) + n_j(t) - 2e_{ij}(t)}\right).$$

The adjacency matrix is updated until the edge weights no longer change, with the limitation that edge weights are permitted only one alteration. After the model is implemented, any weights which fall below the threshold that was used to originally generate the network are set to zero and the resulting change in global efficiency (ΔGE) and size of the giant component (ΔGC) are calculated. We applied the disruption propagation model individually to each node of the fear and control functional connectomes to obtain ΔGE and ΔGC values for each brain region. The model was implemented in R (version 3.2.2) using igraph (version 1.0.1) (Csardi and Nepusz, 2006).

To explore the parameter space of the model, we varied the number of edge weight changes and thresholds for removing edges following propagation in the fear memory network. We used the Shannon's entropy (H) for both ΔGE and ΔGC to determine the information content of the model output. H was calculated using the Entropy package (version 1.2.1) (Hausser and Strimmer, 2009) by discretizing the data into 50 bins ranging from 0 to the maximum value for each measure.

Anatomical network analysis

The mouse anatomical connectome was obtained from Oh et al. (2014), which uses the Allen Brain Atlas (ABA) to define brain regions. Our fear memory network was based on the brain atlas from Paxinos and Franklin (2004). To reconcile these two databases we combined regions to yield a common set of 70 nodes. We used two approaches to generate anatomical networks that were equivalent in different ways to the fear memory functional connectome.

In the first approach, we generated networks that were thresholded using the same p value as used to generate the fear memory connectome ($p < 0.01$). After thresholding, the ipsilateral and contralateral anatomical networks were combined. Next, nodes in both

networks were combined such that the same brain regions were represented resulting in 70 nodes. Edges from combined nodes were averaged to generate the final edge weights.

The above approach to analyze the anatomical networks resulted in very different network densities (functional: 0.08, anatomical: 0.21). Therefore, in a second approach, we generated functional and anatomical networks of approximately equal densities. We generated the anatomical network by first combining ipsilateral and contralateral regions, then thresholded the network by retaining edges with the highest weights such that the network had the same density as the functional network (0.08). In both approaches, unweighted centrality metrics were then calculated as described above.

In order to apply the disruption propagation model to the anatomical network, we set all edge weights in the network to one. Next, we applied the model limiting the edge updates to one and using final cut-off thresholds ranging from 0 to 0.99 at intervals of 0.01. For each threshold, we calculated the Shannon's entropy (H) as described above and chose the threshold value that resulted in maximal entropy for each network.

Cascading failure model

The cascading failure model described in Crucitti et al. (2004) was implemented in R (version 3.2.2) using both the igraph (version 1.0.1) and sna (version 2.3.2) packages (Butts, 2008). Critical tolerance values ($\alpha_{critical}$) were defined as tolerance values that resulted in the largest increase in global efficiency as the tolerance was increased.

Virus

To silence neurons, we used a replication-defective herpes simplex viral vector (HSV) expressing the inhibitory DREADD receptor, hM4Di (kindly provided by Bryan Roth, UNC), along with a fluorescent marker (mCherry). Expression of hM4Di was driven by an EF1α (Human elongation factor-1 alpha) promoter such that long-term (> 4 weeks) expression of the transgene is achieved. HSV virus was packaged using a replication-defective helper virus, purified on a sucrose gradient, pelleted and resuspended in 10% sucrose, as previously described (Rashid et al., 2016; Richards et al., 2014). The average titer of the virus stocks was 4.0×10^7 infectious units/ml. We observed high transgene expression 3 d following microinjection of this virus.

Surgery

Mice were pre-treated with atropine sulfate (0.1 mg/kg, ip), anesthetized (chloral hydrate, 400 mg/kg, ip) and placed in a stereotaxic frame. Viral vectors were bilaterally microinjected (1.5-2.0 μl/side, 0.1 μl/min) into the target region (see Table S2 for region coordinates) via glass micropipettes connected via polyethelene tubing to a microsyringe (Hamilton, Reno, NV). Micropipettes remained in place for 5 min after microinjection to ensure vector diffusion. Mice were treated with analgesia (ketoprofen, 5 mg/kg, sc) following surgery. Behavioral training began 7 d after surgery.

Contextual fear training and testing

Contextual fear conditioning was conducted in stainless steel chambers (31 cm X 24 cm X 21 cm; Med Associates, St. Albans, VT). The floor consisted of stainless steel bars (diameter 3.2 mm) spaced 7.9 mm apart, through which a mild footshock could be delivered. The front, top and back of the chamber were made of clear acrylic and the two sides made of modular aluminum. Behavior was monitored via overhead cameras. An automated scoring system (Freezeframe software; Actimetrics) digitized the video signal at 4 Hz and compared frame by frame movement to determine the amount of time spent freezing. Mice were handled for 5 min/day for 3 days before training. During training, mice were placed in the conditioning chamber for a total of 5 min. After two min, 3 unsignaled footshocks were presented (2 s duration, 0.6 mA, 1 min apart). Following the last footshock, mice remained in the chamber for an additional min, and then returned to their home cage. Memory was tested 10 days after training by placing mice back in the chamber for 5 min while freezing was assessed.

CNO treatment

Immediately after training, mice were systemically administered CNO (5 mg/kg, i.p., Toronto Research Chemicals) or VEH, depending on treatment group. CNO was first dissolved in 20 μL DMSO (Dimethyl sulfoxide, Sigma), then mixed into 380 μL 1 × PBS. Mice assigned to the VEH condition received an injection of 20 μL DMSO mixed with 380 μL 1 × PBS. After CNO or VEH injection, mice were returned to their home cage where CNO (5 mg/kg) or VEH was delivered via drinking water for 10 days. The CNO dose in drinking water was determined based on the amount of water consumed by mice in one day. No other water was available during this time. To assess whether CNO alone impacts fear conditioning, we infused a control virus (HSV-EF1α-GFP) into the CA1 region, administered VEH or CNO, and subjected mice to fear conditioning as described above (N = 8 mice/group).

Verifying viral infections

Following testing in contextual fear conditioning, mice were deeply anesthetized with chloral hydrate and perfused transcardially with PBS followed by 4% paraformaldehyde (PFA). Brains were removed, fixed overnight in PFA, then transferred to 30% sucrose solution and stored at 4°C. Coronal brain slices (50 μm) were collected across the anterior-posterior extent of the injected region. Mice were included in subsequent data analysis only if robust bilateral mCherry expression in the target region was observed in at least 5 consecutive brain sections (across anterior-posterior axis). To determine the percent infected ($mCherry^+$) cells within a

given target region, we traced the target region across 15 serial sections in a set of randomly-selected brains (at least N = 2 per region) then counted the number of mCherry$^+$ neurons within this specific region of interest (ImageJ software, NIH).

In vivo assessment of chemogenetic inhibition

In the present series of experiments, we delivered CNO to mice via drinking water. Drinking is reduced, but not absent, in the inactive phase of the light-dark cycle in mice (Gordon et al., 1986). To test whether CNO administered in drinking water inhibits the activity of neurons expressing hM4Di at different times throughout the light-dark cycle, we microinjected HSV-hM4Di-mCherry bilaterally into the anterior cingulate cortex of mice. Three days later, mice received CNO or VEH in drinking water for 3 consecutive days. Mice were trained in context fear conditioning (as above, 3 footshocks, 0.6 mA, 2 s, 1 min apart) at Zeitgeber time 0, 6, 12 or 18 (N = 3-8 mice/group), and were perfused 90 min after training. Brains were collected and processed for Fos immunohistochemistry. We observed that, despite being trained at different points in the light-dark cycle, CNO always reduced neuronal activation in neurons expressing hM4Di.

Using the same protocol, we tested whether 3 days of CNO treatment decreased neuronal activity in neurons infected with HSV-hM4Di in other brain regions (CA1, LD and MGM, N = 3-5 mice/group). For this experiment, mice were trained at ZT 6 and perfused 90 min later to assess the levels of Fos in infected neurons. In an additional experiment, we tested the effect of 10 days of CNO administered in drinking water (matching the time course of the main experiments) in CA1 infected neurons (N = 4 mice/group). We observed a similar reduction of neuronal activation in all brain regions analyzed irrespective of the number of days CNO was administered.

Immunohistochemistry

To examine Fos protein levels across brain regions, coronal brain slices were incubated with blocking solution (0.1% BSA, 2% NGS, 0.3% Triton X-100) for 2 hr at room temperature, then with anti-c-Fos primary rabbit antibody (1:1000, SC-52; Santa Cruz Biotechnology, Santa Cruz, CA) for 24 hr. Sections were washed, incubated with anti-mouse Alexa 488 secondary antibody (1:500, Invitrogen) for 2 hr at room temperature. Sections were washed, mounted on slides and coverslipped using PermaFluor mounting medium. Nuclei were counterstained with DAPI (Vectashield, Vector Labs Burlingame, CA). Images were obtained using a confocal laser scanning microscope (LSM 710; Zeiss).

QUANTIFICATION AND STATISTICAL ANALYSIS

Statistical details, such as number of mice used in different experiments can be found in the results and methods sections. Group data are presented as mean ± SEM. Mice were included in the analysis only if robust viral expression was observed as described above. Pearson's correlations (r) were calculated using R (version 3.2.2) or Prism 5.

Fos level quantification

t tests or 2-ways ANOVAs were used to analyze Fos levels as described in the results section using Prism 5.

Permutation testing

We conducted permutation testing to determine the level of significance of the difference in freezing in CNO- versus VEH-treated mice. Permutation testing was performed by resampling the freezing data from all 21 experiments without replacement and shuffling drug (CNO versus VEH) and brain region 1000 times. After each resampling, Δfreezing was recalculated for each brain region, resulting in a distribution of Δfreezing values that was used to calculate a p value for each of the 21 experiments. To correct for the inclusion of 21 individual experiments, we adjusted the resulting p values using an FDR of 5% using the Benjamani and Hochberg procedure as implemented in R (version 3.2.2) (Benjamini and Hochberg, 1995).

DATA AND SOFTWARE AVAILABILITY

The accession number for the data associated with each figure, and code for the disruption propagation and cascading failure models reported in this paper, is Dryad: 86337.